Title: The odor of a nontoxic tetrodotoxin analog, 5,6,11-trideoxytetrodotoxin, is detected by specific olfactory sensory neurons of the green spotted puffers but is processed in overlapping olfactory bulbar area with food odors.

Authors: Takehisa Suzuki[1], Ryota Nakahigashi[2], Masaatsu Adachi[2†], Toshio Nishikawa[2], and Hideki Abe[1*]

Affiliations

1. Laboratory of Fish Biology, Graduate School of Bioagricultural Sciences, Nagoya University, Furo-cho, Chikusa-ku, Nagoya, Aichi 464-8601, Japan
2. Laboratory of Organic Chemistry, Graduate School of Bioagricultural Sciences, Nagoya University, Furo-cho, Chiku-ku, Nagoya, Aichi 464-8601, Japan

† Present address: Laboratory of Heterocyclic Chemistry, Graduate School of Pharmaceutical Sciences, Tohoku University, 6-3 Aoba, Aramaki, Aoba-ku, Sendai 980-8578, Japan

Corresponding author's address

Hideki Abe

Laboratory of Fish Biology, Graduate School of Bioagricultural Sciences,

Nagoya University, Furo-cho, Chikusa-ku, Nagoya, Aichi 464-8601, Japan

habe@agr.nagoya-u.ac.jp

Keywords

electroporation, toxification, calcium imaging, feeding, chemical communication

Abstract (207/250 words)

Toxic puffers accumulate tetrodotoxin (TTX), a well-known neurotoxin, by feeding on TTX-bearing organisms and using it to defend themselves from predators. Our previous studies have demonstrated that toxic puffers are attracted to 5,6,11-trideoxytetrodotoxin (TDT), a nontoxic TTX analog that is simultaneously accumulated with TTX in toxic puffers and their prey. In addition, activity labeling using immunohistochemistry targeting neuronal activity marker suggests that TDT activates crypt olfactory sensory neurons (OSN) of the green spotted puffer. However, it remains to be determined whether individual crypt OSNs can physiologically respond to TDT and whether TDT is processed differently from other odors in the brain. By employing electroporation to express GCaMP6s in OSNs, we successfully identified a distinct group of oval OSNs that exhibited a specific calcium response when exposed to TDT in green spotted puffers. These oval OSNs showed no response to amino acids (AAs), which serve as food odor cues for teleosts. Furthermore, immunohistochemistry targeting neural activity markers revealed that TDT and AAs odors activate extensively overlapping areas in the dorsomedial olfactory bulb. These results suggest that while different types of OSNs detect TDT and AAs in the olfactory epithelium, these substances are processed as similar odors in the olfactory bulb. The TDT odor may act as a chemoattractant for finding conspecific toxic puffers and for feeding TTX-bearing organisms for effective toxification.

Introduction

Tetrodotoxin (TTX) is a well-known neurotoxin found in toxic puffers that blocks sodium channels and prevents the generation and conduction of nerve impulses, leading to paralysis and potentially fatal respiratory and cardiac failure. Toxic puffers accumulate TTX in their bodies by feeding on TTX-bearing organisms and using it to defend themselves from predators (Noguchi et al. 2006). While some studies have suggested that TTX attracts toxic puffers through olfaction (Matsumura 1995; Okita et al. 2013), our electrophysiological and behavioral study has demonstrated that the grass puffer *Takifugu alboplumbeus* is attracted to 5,6,11-trideoxyTTX (TDT), a nontoxic TTX analog that is accumulated simultaneously with TTX in toxic puffer or their prey (Noguchi et al. 2022). Furthermore, our behavioral and immunohistochemical study also revealed that TDT attracts the green spotted puffer *Dichotomyctere nigroviridis*, which is phylogenetically and geographically quite different from the genus *Takifugu*, and then activates crypt olfactory sensory neurons (OSNs) (Suzuki et al. 2022). Based on these studies, we hypothesized that TDT, an attractive odorant in toxic puffers, is detected by crypt OSNs. However, we have yet to establish whether single crypt OSNs can physiologically respond to TDT and whether TDT is processed differently from other odors in the brain.

In this study, we demonstrated the response of OSNs to TDT in green spotted puffers by expressing GCaMP6s, a genetically encoded calcium indicator. To achieve this, we used *in vivo* electroporation to perform transient exogenous gene transfer into the olfactory epithelium (OE), leveraging the unique anatomical features of the nasal organ of the green spotted puffer that protrudes from the body surface. As a result, OSNs that responded to TDT (= crypt-type OSNs) odor did not respond to amino acids (AAs). Conversely, OSNs that responded to AAs did not respond to TDT, indicating that different OSNs detect them. However, when the olfactory bulbar (OB) areas activated by these odors were verified using

immunohistochemistry against neural activity markers, it was found that both TDT and AAs activated extensively overlapping areas of the dorsomedial OB. Until now, crypt-type OSNs were believed to process odor information related to social behaviors such as reproductive behaviors (Bazáes and Schmachtenberg 2012) and kin recognitions (Biechl et al. 2016). However, considering our present results and the fact that toxic puffers preferentially prey on TTX-bearing organisms (Ito et al. 2023; Itoi et al. 2015; Okabe et al. 2019), it is speculated that TDT is processed as a chemoattractant for finding conspecific toxic puffers and for feeding TTX-bearing organisms for effective toxification.

Materials and Methods

Animals

Green spotted puffers (*Dichotomyctere nigroviridis*; standard body length:1.5–3.0 cm, bodyweight:0.5–1.5 g) were purchased from a local dealer and maintained in 60 L tanks (28°C; 20–30 fish per tank) filled with artificial brackish water (ABW; Instant Ocean Sea-Salt, Cl^- 543 mM, Na^+ 471 mM, Mg^{2+} 54.3 mM, K^+ 10.7 mM, Ca^{2+} 10 mM, Br^- 0.7 mM, Sr^{2+} 0.1 mM, F^- 0.05 mM, I^- 0.002 mM, CO_3^{2-}/HCO_3^- 3.3 mM, pH 8.2; Instant Ocean, Blacksburg, VA) with a specific gravity of 1.010 under a 12 h light/12 h dark photoperiod. The fish were fed dried shrimp once a day. Since it is difficult to determine sex and sexual maturity from appearance, several fish were anesthetized with tricaine methane sulfonate (MS-222; 0.02%, Sigma-Aldrich, St. Louis, MO), and their gonads were dissected. All fish identified were juveniles with immature gonads; therefore, both males and females were used without distinction in this study. The animal use and care protocols were approved by the Center for Animal Research and Education of the Nagoya University (approved number: A210871-004). All animals were maintained and used in accordance with the Tokai National Higher Education and Research System Regulations on Animal Care and Use in Research

(Regulation no. 74). No statistical methods were used to predetermine the sample size because many of the outcomes were unknown.

Plasmid

The plasmid containing the medaka β-actin promoter and GCaMP6s was constructed by modifying of *pT2Olactb:loxP-dsR2-loxP-EGFP* plasmid (Yoshinari et al. 2012; a gift from Dr. Masato Kinoshita). The dsR2-loxP-EGFP sequence between the Spe I and Not I sites of *pT2Olactb:loxP-dsR2-loxP-EGFP* was replaced with the *GCaMP6s* sequence, which was obtained as Spe I and Not I fragments from *pGP-CMV-GCaMP6s*. *pGP-CMV-GCaMP6s* was a gift from Douglas Kim & GENIE Project (Chen et al. 2013; Addgene plasmid # 40753 ; http://n2t.net/addgene:40753 ; RRID:Addgene_40753). The purified plasmid was prepared using the NucleoBond® Xtra Midi kit (MACHEREY-NAGEL, Düren, Germany) or the Genopure Plasmid Midi kit (Roche Diagnostics GmbH, Mannheim, Germany). The prepared plasmid was dissolved in TE buffer to 5 μg/μL and stored at -20ºC until use.

In vivo electroporation to the olfactory epithelium of green spotted puffer

The fish were first anesthetized with 0.02% MS-222, and excess water was wiped off. Then, 2 μL of a plasmid solution (1μg/μL) diluted in PBS was administered. The olfactory organ was positioned between self-made tweezer-style silver chloride/silver plate electrodes. The gap between the electrodes was adjusted to 2-3 mm, and square-current pulses were delivered to the olfactory organ using an electronic stimulator (SEN-7203; Nihon Kohden, Tokyo, Japan) through an isolator (SS-202J; Nihon Kohden) at room temperature.

A two-step pulse protocol was used for gene transfer. This protocol comprised an initial high-current single-shot poring pulse with parameters of amplitude (10 mA) and duration (5 ms), followed by multiple low-current transfer pulses (Fig. 1). The pulse parameters,

including the interval between the poring and transfer pulse patterns (20 ~ 1000 ms), amplitude (0.5 ~ 2.0 mA), and frequency (5 ~ 20 Hz) of the transfer pulses, were optimized as described below.

Following electroporation, the fish were allowed to recover for 24-36 h in fresh ABW before use in the experiments. Gene transfer performance was evaluated as the rate of OSNs expressing GCaMP6s per OSNs counted using 4,6-diamidino-2-phenylindole (DAPI) staining normalized to the OE area (90×90 μm^2). To ensure accurate quantification of living OSNs, we included only those cells located within the sensory epithelial layer and exhibiting GCaMP6s fluorescence. Cells that overexpressed fluorescent proteins or exhibited any morphological changes indicative of damage or cell death were excluded.

Odorant solutions

A mixture of amino acids (AAs), including L-arginine, L-glutamine, L-phenylalanine, and L-isoleucine (Sigma-Aldrich), was dissolved in ultrapure water to a concentration of 10^{-4} M and stored as a stock solution at −30°C until use. TDT was synthesized and purified by HPLC using an ion-exchange column (Hitachi gel 3013C). The synthesized TDT was confirmed free of other TTX analogs and reagents, as verified by their ^{1}H and ^{13}C NMR spectra. The purification procedure has been outlined in detail by Adachi et al. (2014). TDT was dissolved in ultrapure water at 10^{-3} M concentration and stored as a stock solution at −30°C until use.

For puff application, all stock solutions were diluted with artificial cerebrospinal fluid for teleosts (ACSF) comprising NaCl (140 mM), KCl (5 mM), $MgCl_2$ (1.3 mM), $CaCl_2$ (2.4 mM), HEPES (10 mM), and glucose (10 mM), and adjusted to pH 7.4 to obtain a working concentration of 10^{-6} M.

Calcium imaging

Electroporated fish were anesthetized with 0.02% MS-222, and the bilateral olfactory organs were excised and halved with a fine blade. The halved olfactory organ was transferred to a recording chamber and anchored with a handmade platinum slice anchor with parallel nylon threads (0.040 - 0.049 mm thickness; C-23S-N5 #8-0, Natsume-Seisakusyo, Tokyo, Japan). The preparation was continuously perfused with ACSF at a rate of 1 mL/min using a peristaltic pump (SJ1211-L, ATTO, Tokyo, Japan) and a vacuum pump (DAL-5s, ULVAC KIKO, Inc., Miyazaki, Japan).

A puff micropipette (with a tip diameter of 2 μm) filled with an odorant solution was carefully positioned 30-50 μm away from the OSN expressing GCaMP6s using a micromanipulator (EMM-3SV, Narishige, Tokyo, Japan) under a fluorescence microscope (Eclipse E600-FN, Nikon, Tokyo, Japan). The microscope was equipped with a 60× water immersion objective lens (CFI Fluor 60X/1.00W; Nikon), a fluorescence filter cube (excitation filter 450~490nm, dichroic mirror 505 nm, and emission filter 520 nm; model B-2A, Nikon), and a CMOS camera (Chamelon3 CM3-U3-31S4M-CS, Teledyne FLIR LLC., Wilsonville, OR).

Puff application of the odorant solutions to OSN was performed by applying air pressure (0.8 kg/cm^2; 500 ms duration; generated by an air compressor) to the puff micropipette using a solenoid valve (UMG1-T1, CKD, Komaki, Aichi, Japan). Time-lapse image acquisition (2 frames/s for 90 s) and puff application were controlled by Micromanager (Edelstein et al. 2014) and Arduino UNO (http://Arduino.cc). After recording, the morphologies of GCaMP6s-expressing OSNs that recorded calcium responses were confirmed using a confocal laser microscope (FV1000D IX81, Olympus, Tokyo, Japan). The fluorescence change was calculated as $\Delta F/ F_0= (F_t – F_0)/F_0$, where F_t is the fluorescence intensity at a given time point, and F_0 is the baseline (the average intensity of the first 10 frames). Time-lapse images were analyzed using Fiji (https://fiji.sc/; Schindelin et al. 2012) and Igor Pro 9.01 (WaveMetrics,

Portland, OR).

Immunohistochemistry

Fish were allowed to acclimate to the aquarium filled with ABW (100 mL) prepared from deionized water and Instant Ocean Sea-Salt for 1h. After acclimation, 1 mL of 1×10^{-4} M odorant solution (vehicle [ABW], AAs, or TDT; diluted with ABW) was gently administered into the aquarium using a 1 mL syringe via a polyvinyl chloride tube (the administration rate was approximately 0.1 mL/s). After 15 min, the fish was promptly anesthetized with 0.1% MS-222 and perfused through the heart with 4% paraformaldehyde in 0.1 M phosphate buffer. The brain was removed from the skull and postfixed in a fresh solution of the same fixative overnight at 4°C, rinsed in PBS, and cryoprotected in 20% sucrose in PBS overnight at 4°C. The brain was embedded in 5% agarose (A2576; Sigma-Aldrich). Transverse cryosections (40 μm) of the brain were mounted onto gelatin-coated slides and dried. After rehydration in PBS, the sections were blocked with 2% normal goat serum in PBS with 0.05% Tween-20 (PBST) for 3 h at 28°C. These sections were incubated successively in PBST with; 1) primary antibodies for 2 days at 4°C; 2) an Alexa Fluor 488-conjugated secondary antibody (goat anti-rabbit IgG [H + L], A-11008, Thermo Fisher Scientific, 1:500) for 1 day at 4°C; and 3) DAPI (1:1,000 dilution) for 5 min at room temperature. The sections were rinsed for 5 min 3 times in PBST after each incubation step, mounted in a mounting medium (10% Mowiol 4-88, 25% glycerol, 0.2 M Tris–HCl [pH 9.0], and 2.5%–3.0% 1,4-diazabicyclo [2,2,2] octane; diluted with ultrapure water), and cover-slipped.

Dendrites were labeled with an anti-microtubule-associated protein 2 (MAP2) mouse monoclonal antibody (M1406, Sigma-Aldrich, 1;500), which was used in zebrafish dendrites, as validated by Becker et al. (2019) as a dendritic marker. Odorant-responsive cells were labeled with an anti-phosphorylated ribosomal protein S6 (pS6) rabbit polyclonal antibody

(Ser244, Sers247 anti-pS6, 44-923G, Thermo Fisher Scientific, MA; 1:5,000), which was used in mouse OSNs (Sharma et al. 2017) and green spotted puffer OSNs (Suzuki et al. 2022), as a neural activity marker.

Optical sections of the immunohistochemistry and DAPI–stained OEs were acquired using an FV1000D IX81 confocal laser-scanning microscope (Olympus). All microscopic images used in this study were processed to pseudo color stacks and adjusted for brightness and contrast using Fiji. We sampled every two transverse sections from the rostral to the caudal end of the OB (five sections per animal) and measured the number of pS6-positive cells.

Statistical Analysis

Data are expressed as the mean ± standard error of the mean and represented as a bee swarm plot and box-whisker plot (marker: mean; box: median and quartiles; whiskers: 10%–90% range) or a line plot. Igor pro 9 (WaveMetrics Inc., Lake Oswego, OR) and JASP (JASP team, 2023; Version 0.17.2) were used for statistical analysis and graph preparation.

Results

Optimization of Electroporation Conditions for Transient Gene Transfer to Olfactory Sensory Neurons

To investigate the physiological response of OSNs to TDT, we used a transient gene transfer method using *in vivo* electroporation to express GCaMP6s in the OSNs of green spotted puffers. Initially, we applied a train of square-current pulses (5 pulses, 50 ms duration, 10 Hz frequency, and 0.5 mA current amplitude; transfer pulse; Table 1) to the OE of green spotted puffers following dropwise addition of the GCaMP6s plasmid solution. The resulting

GCaMP6s expression rate within a particular area (90×90 μm^2) of the OE was 0.09 ± 0.01% (n = 6; measured 24~36h after electroporation; Fig. 2Aa).

To enhance the efficiency of gene transfer, we implemented a two-step current-pulse protocol consisting of an initial high-current, single-shot poring pulse (10 mA, 5 ms) followed by five low-current transfer pulses (0.5 mA, 50 ms, and 50% duty cycle; Fig. 1). By adjusting the interval between the two pulse patterns, we observed an increase in the GCaMP6s expression rate, but no significant difference was observed (0.09 ± 0.01%, n = 6, transfer pulse only; 0.61 ± 0.38%, n = 6, 20 ms interval; 0.26 ± 0.20%, n = 6, 100 ms interval; 0.17 ± 0.12%, n = 6, 1000 ms interval; Fig. 2Aa). Therefore, we connected the poring pulse and transfer pulses at an interval of 20 ms and set the poring pulse waveform (10 mA, 5 ms) and transfer pulse duty cycle (50%) to be constant for subsequent experiments.

Next, we investigated the effect of the transfer pulse frequency by changing the pulse duration while maintaining the amplitude of the transfer pulse at 1.0 mA. The GCaMP6s expression rate at 20 Hz transfer pulse frequency was significantly higher than those of 5 Hz or 10 Hz (0.79 ± 0.29% at 5 Hz, n = 6; 0.61 ± 0.23% at 10 Hz, n = 6; 2.36 ± 0.41% at 20 Hz, n = 6; P = 0.906 for 5 Hz vs. 10 Hz, P = 0.005 for 5 Hz vs. 20 Hz, and P = 0.002 for 10 Hz vs. 20 Hz; Fig. 2Ab). Additionally, when we varied the amplitude of the transfer pulse while maintaining the poring pulse waveform and the frequency of the transfer pulse constant, the GCaMP6s expression rate tended to increase from 1.15 ± 0.29% at 0.5 mA to 2.41 ± 0.40% at 1.0 mA (n = 10, respectively), although the increases was not statistically significant (P = 0.063). However, further increasing the transfer pulse amplitude to 2.0 mA led to a decrease in the expression rate to 1.10 ± 0.47% and resulted in the rupture and death of many OSNs (P = 0.994 vs. 0.5 mA, P = 0.052 vs. 1.0 mA; Fig. 2Ac). The changes in GCaMP6s expression rate under these conditions are summarized in Table 1.

Based on these results, we employed a two-step pulse protocol consisting of a 5 ms

poring pulse with a 10 mA current amplitude, followed 20 ms later by five transfer pulses with a 1.0 mA current amplitude and 25 ms duration at 50% duty cycles. *In vivo* electroporation using these parameters resulted in scattered GCaMP6s-expressing OSNs on the OE of green spotted puffers at a density where individual cell shapes could be distinguished (Fig. 2B).

<u>OSNs exhibit specific calcium responses to amino acids or TDT.</u>

Using electroporated OE, we investigated the physiological response of individual OSNs to odorants by detecting fluorescence changes in GCaMP6s. Puff administration of a 10^{-6} M mixture of four amino acids (L-Arginine, L-Glutamine, L-phenylalanine, and L-Isoleucine; AAs), which are known to act as odorants in many fish, induced a transient intracellular Ca^{2+} increase in GCaMP6s-expressing OSNs. In contrast, when we administered ACSF as a vehicle control, no response was observed (Fig. 3A). These results were consistent across several repetitions, with the peak amplitudes of the Ca^{2+} response (expressed as $\Delta F/F_0$; %) induced by AAs significantly greater than those of the vehicle (9.59 ± 3.88% for AAs vs. 0.63 ± 0.26% for the vehicle (n = 14), P = 0.00032; Fig. 3B). After calcium imaging, we confirmed the morphology of AAs-responsive OSNs using confocal laser microscopy. The AAs-responsive OSNs exhibited spindle-shaped morphology with a short diameter of approximately 4 μm. Their cell bodies were located slightly deeper on the OE surface (Fig. 3C). TDT-sensitive OSNs also exhibited a transient increase in Ca^{2+}. The amplitudes were significantly higher than the vehicle's (16.21 ± 3.10% for TDT vs. 1.07 ± 0.13% for the vehicle, n = 16, P = 0.00014; Fig.3D and E). These TDT-sensitive OSNs exhibited oval-shaped morphology with a short diameter of approximately 6 μm, and their cell bodies were located on the surface of the OE (Fig. 3F).

We further examined the response of TDT-sensitive OSNs to AAs and vice versa. Regardless of the order of application, TDT-sensitive OSNs did not exhibit any fluorescence

increase following the application of the vehicle or AAs (0.94 ± 0.09% for the vehicle vs. 8.51 ± 2.18% for TDT, P = 0.005; the vehicle vs. 0.71 ± 0.24% for AA, P = 0.901; TDT vs. AAs, P = 0.005, n = 6, respectively; Fig. 4A and B). Similarly, AAs-sensitive OSNs did not display any fluorescence increase by application of TDT or the vehicle (0.79 ± 0.39% for the vehicle vs. 0.38 ± 0.06% for TDT, P = 0.786; the vehicle vs. 7.47 ± 0.55% for AAs, P = 0.002; TDT vs. AAs, P = 0.002, n = 6, respectively; Fig. 4C, and D). Notably, no OSNs were observed to respond to both odorants, AAs and TDT.

TDT and AAs activated extensively overlapped neuronal populations in the olfactory bulb

Individual OSNs express a single type receptor for specific odorant molecules, and their axons converge onto a dedicated glomerulus within the OB. To investigate whether TDT and other odorants converge into different glomerulai within the OB, we analyzed the structure of the green spotted puffer's OB using immunohistochemistry with a dendritic marker, MAP2 antibody, and nuclear staining with DAPI. The nuclei were distributed across the surface (especially the ventral surface) and dorsomedial areas of the OB (Fig. 5B). Within the dorsomedial area, we observed a high density of nuclei forming distinct layers (Fig. 5B-2,3,4). Moreover, their dendrites span from the rostral (Fig. 5C-1) to the ventrolateral surface, covering the center of the OB (Fig. 5C-3,4,5). These results suggest that the axons of OSNs project towards the center of the OB, and the dendrites of granule or mitral cells envelop them, forming glomeruli.

To investigate whether axons of TDT- or AAs-activated OSNs activate different OB areas, we immunohistochemically labeled odorant-activated OB cells using a pS6 antibody as a marker for neuronal activity. TDT-activated cells were densely located in the rostral and caudal region of the dorsomedial OB (dm; Fig. 6B-1,4,5). In contrast, AAs-activated cells

were present in both the dm and the ventrolateral (vl) OB (Fig. 6C). Many of the activated area within dm OB overlapped with the area activated by TDT. However, TDT-activated cells were distributed more dorsally (Fig. 6B-4, 5), and the AAs-activated cells were distributed more ventrally (Fig. 6C-4, 5) in the caudal region of dm OB. In the case of the vehicle administration, only a few cells were observed in the dm OB (Fig. 6D). The density of pS6-positive cells was quantified by counting the number of cells within a square area of 100 μm in the dm and vl (n = 4). The number of cells responding to TDT was higher in dm than in vl across the rostrocaudal axis of OB. Significant differences were observed in the rostral (63.5 ± 8.3 cells/10^4 μm in dm-1 vs. 11.5 ± 4.8 cells/10^4 μm in vl-1, P = 0.001) and caudal dm (53.8 ± 13.5 cells/10^4 μm in dm-4 vs. 12.5 ± 3.7 cells/10^4 μm in vl-4, P = 0.036; 61.3 ± 12.2 cells/10^4 μm in dm-5 vs. 9.3 ± 5.5 cells/10^4 μm in vl-5, P = 0.001; Fig. 6Ea). AAs and the vehicle activated more cells in the dm than in the vl, but no significant differences were observed (Fig. 6Eb, Ec). When comparing the number of pS6-positive cells in the dm and vl along the rostrocaudal axis, both AAs and TDT significantly activated more cells than the vehicle at the most rostral sections of the dm (63.3 ± 5.2 cells/10^4 μm in AAs vs. 16.5 ± 8.0 cells/10^4 μm in the vehicle, P = 0.020; 63.5 ± 8.3 cells/10^4 μm in TDT vs. 16.5 ± 8.0 cells/10^4 μm in the vehicle, P = 0.018; Fig.6Fa-1). In the caudal section, only TDT significantly activated more cells than the vehicle (47.5 ± 14.3 cells/10^4 μm in AAs vs. 17.3 ± 3.2 cells/10^4 μm in the vehicle, P = 1.000; 61.3 ± 12.2 cells/10^4 μm in TDT vs. 17.3 ± 3.2 cells/10^4 μm in the vehicle, P = 0.044; Fig.6Fa-5). In contrast, in the vl, AAs activated more cells than the vehicle and TDT along the rostrocaudal axis, but there was no significant difference between them (Fig.6Fb). These results suggest that both TDT and AAs activate broad areas of the OB, but TDT mainly activates the caudal region of the dm OB. In contrast, AAs mainly activate the rostral region of the dm OB and, although not significantly different, the vl surface of the OB. These suggest that odor information about TDT and AAs is detected by distinct OSNs,

but is processed through extensively overlapping pathways from the OE to the OB.

Discussion

In this study, we demonstrated that oval OSNs, possibly crypt-type OSNs as inferred from our previous morphological studies, specifically respond to TDT. In contrast, the activation of these OSNs by TDT activates the broad area of the dorsomedial OB that is extensively overlapped with the area activated by the AAs, which are food odors for teleosts.

To investigate whether live OSN of green spotted puffer detects TDT, we expressed GCaMP6s in the OSNs by *in vivo* electroporation. This technique was necessary to introduce exogenous genes to the OE of the green spotted puffer, as it is challenging to use transgenic techniques due to difficulties with lab-based breeding. The OE of green spotted puffer has notably advantageous features for *in vivo* electroporation. Because the teleosts olfactory organs are generally located in nasal cavities beneath the body surface (Olivares and Schmachtenberg 2019), green spotted puffers have olfactory organs that protrude from the dorsal head surface, exposing the OE to the external environment (cf. Fig.6B of Suzuki et al. 2022). This facilitates the administration of DNA solutions and the positioning of electrodes for electroporation.

The parameters of the electroporation pulse, such as waveform (exponential decay or square wave), pulse amplitude, duration, number, and frequency, are critical for optimizing gene transfer efficiency while maintaining target cell's physiological activity (Young and Dean 2015). We used a two-step constant-current pulse, combining a high-current, short-duration poring pulse with low-current, long-duration transfer pulses to introduce plasmid DNA into OSNs. Sadik et al. (2014) reported that a two-step pulse, combining the first large pulse and subsequent small pulses, can improve gene delivery efficiency and maintain cell viability. Another critical aspect is using constant-current pulses instead of constant-voltage

pulses, which are more commonly employed in other electroporation procedures. With constant-voltage pulses, the current amplitude decays during the pulse, whereas with constant-current pulses, the driving force on the charged molecules remains constant, even if the tissue's resistance changes during the current flow (Draghia-Akli et al. 2008). The disadvantage of electroporation is that the gene transfer efficiency is lower than other exogenous gene delivery methods. However, the sparse gene expression in the OE was advantageous for recording odorant responses from single OSNs, as it allows for better identification of individual cell morphology. For these reasons, our two-step constant-current in vivo electroporation of GCaMP6s is an adequate method for the visualization of live OSN activity.

Oval-shaped OSNs of green spotted puffers physiologically respond to TDT. These TDT-responsive OSNs did not respond to stimuli like AAs or the vehicle, and we found no OSNs that responded to both AAs and TDT. In teleosts, OSNs are categorized into several types, including ciliated, microvillous, crypt, kappe, and pear-shaped cells (Olivares and Schmachtenberg, 2019). This classification is based on their morphology, the position of their soma within the OE, and the specific olfactory receptor gene families they express (Kermen et al. 2013). Crypt OSNs, characterized by oval-shaped cell bodies with apical invagination, are commonly found in various fish species and positioned in the apical layer of the OE (Hansen and Finger 2000). In our study, TDT-responsive OSNs displayed oval-shaped morphology and were located on the surface of the OE. These morphological characteristics are well in agreement with our previous study, in which we conducted double immunohistochemistry for neuronal activity markers and crypt OSNs markers to TDT-administered OSNs (S100; Suzuki et al. 2022).

Various odorants have been reported as ligands for crypt OSNs, yet the specific category of odor they respond to remains uncertain. In initial physiological experiments using acutely

dispersed OE cells from the Pacific jack mackerel *Trachurus symmetricus*, AAs were reported to activate crypt OSNs (Schmachtenberg 2006; Vielma et al. 2008). A subsequent Ca^{2+}-imaging study by Bazáes and Schmachtenberg (2012) reported that dispersed crypt OSNs of juvenile rainbow trout responded to a broad range of common odorants for teleosts, including AAs, bile salts, and conspecific gonadal extracts from males and females. These gonadal extracts contain reproductive pheromones. However, the crypt OSNs of sexually mature rainbow trout became responsive to only gonadal extracts from the opposite sex, and there was an increase in the number of crypt OSNs located on the OE surface. In addition, crypt OSNs respond to the kin odor, potentially linked to major histocompatibility complex II peptides, in zebrafish *Danio rerio* larva (Biechl et al. 2016), and also responded to prostaglandin E2, a pheromone that triggers synchronous spawning behavior in the surrounding individuals of adult grass puffer (Chen et al. 2022). From these results, it can be inferred that crypt OSNs in mature teleosts play a crucial role in detecting olfactory signals tied to reproductive behaviors. TTX (actually TDT) leaking from the oocytes has been reported to attract male grass puffers at the time of spawning (Matsumura, 1995). Therefore, the TDT is considered to satisfy the criteria for inclusion in the repertoire of biologically relevant odor ligands for crypt OSNs.

TDT activated a broad area of dorsomedial OB. Many of the activated area overlapped those activated by AAs, which are food odors for teleosts, but are partially separated in the caudal region. OB areas that respond to specific odors have been studied in several teleosts, but these response areas vary among species (Bazáes et al. 2013). This may be due to differences in the cell organization of the OB. Many fish OBs show a concentrically laminated structure (Satou 1990); however, OB neurons of the green spotted puffer have a laminar structure biased toward the dorsomedial OB. This structural feature of OB is similar to the *Betta splendens* OB (Horn and Rasia-Fliho 2018) or the caudal part of zebrafish OB

(Kenny et al. 2021). In zebrafish, crypt OSNs are projected to dorsomedial OB (Ahuja et al. 2013; Gayoso et al. 2012; Kress et al. 2015). The TDT-induced activation of dorsomedial OB in green spotted puffer corresponds with the area projected by crypt OSNs in zebrafish.

Previous studies have suggested that toxic puffers accumulate TTX and its analogs in their bodies by feeding preferentially on TTX-bearing organisms (Ito et al. 2023; Itoi et al. 2015; Okabe et al. 2019) and may also be attracted to TDT, leaking with TTX from their ovaries (Noguchi et al. 2022). It has also been suggested that crypt OSNs are involved in detecting TDT (Suzuki et al. 2022). In this study, we found that different types of OSNs detect TDT and AAs in OE, whereas the areas activated by these odors overlap in OB. Previous physiological studies using other fish OBs had shown that AAs activated the lateral OB (Friedrich and Korsching 1997), whereas kin odor detected by crypt OSNs activated different areas (medial OB; Biechl et al. 2017). Crypt OSNs are suggested to be involved in social behavior such as reproduction (Bazáes and Schmachtenberg 2012) or kin recognition (Biechl et al. 2016). The present results suggest that the central nervous system of green spotted puffers may somehow process the TDT odor detected by crypt OSN as a ‘food odor’. This finding is further supported that TDT odor may act as a chemoattractant for finding conspecific toxic puffers and may also serve to feed on TTX-bearing organisms for effective toxification.

Acknowledgments

We would like to express our gratitude to Drs. Shinji Kanda (Univ. of Tokyo) and Chika Fujimori (currently, Hokkaido Univ.) for their suggestions about *in vivo* electroporation. We also thank all the staff of the Laboratory of Fish Biology for their suggestions during the experiment.

Competing interests

The authors declare no competing or financial interests.

Funding

This work was supported by Grants-in-Aid for Scientific Research (19K06762 to H.A., 17K19195 to T.N. and H.A., and 17H06406 to T.N.), SUNBOR GRANT from the Suntory Institute for Bioorganic Research to T.S, and JST SPRING (JPMJSP2125) from "Interdisciplinary Frontier Next-Generation Researcher Program of the Tokai Higher Education and Research System." to T.S.

References

Adachi, M., Sakakibara, R., Satake, Y., Isobe, M., and Nishikawa, T. 2014. Synthesis of 5,6,11-trideoxytetrodotoxin. *Chem Lett*. 43:1719–1721.

Ahuja, G., Ivandić, I., Saltürk, M., Oka, Y., Nadler, W., and Korsching, S.I. 2013. Zebrafish crypt neurons project to a single, identified mediodorsal glomerulus. *Sci Rep*. 3:2063.

Bazáes, A., and Schmachtenberg, O. 2012. Odorant tuning of olfactory crypt cells from juvenile and adult rainbow trout. *J Exp Biol*. 215:1740–1748.

Bazáes, A., Olivares, J., and Schmachtenberg, O. 2013. Properties, projections, and tuning of teleost olfactory receptor neurons. *J Chem Ecol*. 39.

Beckers, A., Van Dyck, A., Bollaerts, I., Van houcke, J., Lefevere, E., Andries, L., Agostinone, J., Van Hove, I., Di Polo, A., Lemmens, K., et al. 2019. An antagonistic axon-dendrite Iinterplay enables efficient neuronal repair in the adult zebrafish central nervous system. *Mol Neurobiol*. 56:3175–3192.

Biechl, D., Tietje, K., Gerlach, G., and Wullimann, M.F. 2016. Crypt cells are involved in kin recognition in larval zebrafish. *Sci Rep*. 6:24590.

Biechl, D., Tietje, K., Ryu, S., Grothe, B., Gerlach, G., and Wullimann, M.F. 2017. Identification of accessory olfactory system and medial amygdala in the zebrafish. *Sci Rep*. 7: 44295

Chen, J., Katada, Y., Okimura, K., Yamaguchi, T., Guh, Y.-J., Nakayama, T., Maruyama, M., Furukawa, Y., Nakane, Y., Yamamoto, N., et al. 2022. Prostaglandin E2 synchronizes lunar-regulated beach spawning in grass puffers. *Curr Biol*. 32:4881-4889.e5.

Chen, T.-W., Wardill, T.J., Sun, Y., Pulver, S.R., Renninger, S.L., Baohan, A., Schreiter, E.R.,

Kerr, R.A., Orger, M.B., Jayaraman, V., et al. 2013. Ultrasensitive fluorescent proteins for imaging neuronal activity. *Nature*. 499:295–300.

Draghia-Akli, R., Khan, A.S., Brown, P.A., Pope, M.A., Wu, L., Hirao, L., and Weiner, D.B. 2008. Parameters for DNA vaccination using adaptive constant-current electroporation in mouse and pig models. *Vaccine*. 26:5230–5237.

Edelstein, A.D., Tsuchida, M.A., Amodaj, N., Pinkard, H., Vale, R.D., and Stuurman, N. 2014. Advanced methods of microscope control using μManager software. *J Biol Methods*. 1:e10.

Friedrich, R.W., and Korsching, S.I. 1997. Combinatorial and chemotopic odorant coding in the zebrafish olfactory bulb visualized by optical imaging. *Neuron*. 18:737–752.

Gayoso, J., Castro, A., Anadón, R., and Manso, M.J. 2012. Crypt cells of the zebrafish *Danio rerio* mainly project to the dorsomedial glomerular field of the olfactory bulb. *Chem Senses*. 37:357–369.

Hansen, A., and Finger, T.E. 2000. Phyletic distribution of crypt-type olfactory receptor neurons in fishes. *Brain Behav Evol*. 55:100–110.

Horn, .C., and Rasia-Filho, A.A. 2018. The cytoarchitecture of the telencephalon of *Betta splendens* Regan 1910 (Perciformes: Anabantoidei) with a stereological approach to the supracommissural and postcommissural nuclei. *Anat Rec*. 301:88–110.

Ito, M., Shirai, K., Oyama, H., Yasukawa, S., Asano, M., Kihara, M., Suo, R., Sugita, H., Nakahigashi, R., Adachi, M., et al. 2023. Geographical differences in the composition of tetrodotoxin and 5,6,11-trideoxytetrodotoxin in Japanese pufferfishes and their origins. *Chemosphere*. 336:139214.

Itoi, S., Kozaki, A., Komori, K., Tsunashima, T., Noguchi, S., Kawane, M., and Sugita, H. 2015. Toxic *Takifugu pardalis* eggs found in *Takifugu niphobles* gut: Implications for TTX accumulation in the pufferfish. *Toxicon*. 108:141–146.

Kenney, J.W., Steadman, P.E., Young, O., Shi, M.T., Polanco, M., Dubaishi, S., Covert, K., Mueller, T., and Frankland, P.W. 2021. A 3D adult zebrafish brain atlas (AZBA) for the digital age. *ELife*. 10:e69988.

Kermen, F., Franco, L.M., Wyatt, C., and Yaksi, E. 2013. Neural circuits mediating olfactory-driven behavior in fish. *Front Neural Circuits*. 7:62.

Kress, S., Biechl, D., and Wullimann, M.F. 2015. Combinatorial analysis of calcium-binding proteins in larval and adult zebrafish primary olfactory system identifies differential olfactory bulb glomerular projection fields. *Brain Struct Funct*. 220:1951–1970.

Matsumura, K. 1995. Tetrodotoxin as a pheromone. *Nature*. 378:563–564.

Noguchi, T., Arakawa, O., and Takatani, T. 2006. TTX accumulation in pufferfish. *Comp Biochem Physiol Part D Genomics Proteomics*. 1:145–152.

Noguchi, Y., Suzuki, T., Matsutani, K., Sakakibara, R., Nakahigashi, R., Adachi, M., Nishikawa, T., and Abe, H. 2022. An almost nontoxic tetrodotoxin analog, 5,6,11-trideoxytetrodotoxin, as an odorant for the grass puffer. *Sci Rep*. 12: 15087.

Okabe, T., Oyama, H., Kashitani, M., Ishimaru, Y., Suo, R., Sugita, H., and Itoi, S. 2019. Toxic flatworm egg plates serve as a possible source of tetrodotoxin for pufferfish. *Toxins*. 11:402.

Okita, K., Yamazaki, H., Sakiyama, K., Yamane, H., Niina, S., Takatani, T., Arakawa, O., and Sakakura, Y. 2013. Puffer smells tetrodotoxin. *Ichthyol Res*. 60:386–389.

Olivares, J., and Schmachtenberg, O. 2019. An update on anatomy and function of the teleost olfactory system. *PeerJ*. 7:e7808.

Sadik, M.M., Yu, M., Zheng, M., Zahn, J.D., Shan, J.W., Shreiber, D.I., and Lin, H. 2014. Scaling relationship and optimization of double-pulse electroporation. *Biophys J*. 106:801–812.

Satou, M. 1990. Synaptic organization, local neuronal circuitry, and functional segregation of the teleost olfactory bulb. *Prog Neurobiol*. 34:115–142.

Schindelin, J., Arganda-Carreras, I., Frise, E., Kaynig, V., Longair, M., Pietzsch, T., Preibisch, S., Rueden, C., Saalfeld, S., Schmid, B., et al. 2012. Fiji: an open-source platform for biological-image analysis. *Nat Methods*. 9:676–682.

Schmachtenberg, O. 2006. Histological and electrophysiological properties of crypt cells from the olfactory epithelium of the marine teleost *Trachurus symmetricus*. *J Comp Neurol*. 495:113–121.

Sharma, R., Ishimaru, Y., Davison, I., Ikegami, K., Chien, M.-S., You, H., Chi, Q., Kubota, M., Yohda, M., Ehlers, M., et al. 2017. Olfactory receptor accessory proteins play crucial roles in receptor function and gene choice. *ELife*. 6:e21895.

Suzuki, T., Nakahigashi, R., Adachi, M., Nishikawa, T., and Abe, H. 2022. Green spotted puffers detect a nontoxic TTX analog odor using crypt olfactory sensory neurons. *Chem Senses*. 47:bjac011.

Vielma, A., Ardiles, A., Delgado, L., and Schmachtenberg, O. 2008. The elusive crypt olfactory receptor neuron: evidence for its stimulation by amino acids and cAMP pathway agonists. *J Exp Biol*. 211:2417–2422.

Yoshinari, N., Ando, K., Kudo, A., Kinoshita, M., and Kawakami, A. 2012. Colored medaka and zebrafish: transgenics with ubiquitous and strong transgene expression driven by the medaka β-actin promoter. *Dev Growth Differ.* 54:818–828.

Young, J.L., and Dean, D.A. 2015. Chapter Three - Electroporation-Mediated Gene Delivery. *In: L. Huang, D. Liu, and E. Wagner, eds*. *Advances in Genetics.* Academic Press. pp. 49–88.

Figure legends

Table 1: Electroporation pulse condition and GCaMP6s expression rate.

Bold indicates the modified parameters.

Fig. 1: Electroporation pulses

Schematic diagram representing the waveform used for electroporation.

Fig. 2: *In vivo* electroporation of GCaMP6s to OSNs.

A: Effect of electroporation parameters.

Effects of the pattern interval between the poring and the transfer pulse (**a**), transfer pulse frequency (**b**), and transfer pulse amplitude (**c**) on the expression rate of GCaMP6s in OSNs. Each condition was repeated for six trials (for pattern interval and transfer pulse frequency) or ten trials (for transfer pulse amplitude). Dunnett's multiple comparison test (in comparison with t. pulses only; for (**a**)) or Tukey's multiple comparison test. **P < 0.01.

B: Confocal microscopy image of GCaMP6s-expressing OSNs in OE electroporated with our employed protocol. Scale bar: 20 µm.

Fig. 3: Response of OSNs to AAs or TDT.

(**A**) Fluorescence changes in AAs-responsive OSNs to the vehicle or AAs exposure. Individual AAs-responsive OSNs (n = 14) are represented by gray dashed lines, with the bold line and envelope showing the mean ± SEM. Representative fluorescence image frames (**a-e**; the vehicle, **f-j**; AAs) indicated by vertical lines are shown above the trace. (**B**) The peak amplitude of AAs-responsive OSNs after administering the vehicle (black) or AAs (brown). Paired t-test compared the vehicle vs. AAs administration. ***P < 0.001. (**C**) Reconstructed confocal image of the AAs-

responsive OSN as depicted in **A**. Scale bar: 2 μm. (**D**) Fluorescence changes in TDT-responsive OSNs to the vehicle or TDT exposure. Individual TDT-responsive OSNs (n = 16) are represented by gray dashed lines, with the bold line and envelope showing the mean ± SEM. Representative frames (**a-e**; the vehicle, **f-j**; TDT) indicated by vertical lines are shown above the trace. (**E**) The peak amplitude of TDT-responsive OSNs after administering the vehicle (black) or TDT (green). Paired t-test compared the vehicle vs. TDT administration. ***P < 0.001. (**F**) Morphology of the TDT-responsive OSN as depicted in **D**. Scale bar: 2 μm.

Fig. 4: TDT-responsive OSNs did not respond to AAs.

(**A**)Fluorescence changes in TDT-responsive OSNs to the vehicle, TDT, and AAs exposure. Individual OSNs (n = 6) are represented by gray dashed lines, with the bold line and envelope indicating the mean ± SEM.

(**B**)Peak amplitude of TDT-responsive OSNs after the administration of the vehicle (black), TDT (green), and AAs (brown). One-factor repeated measures ANOVA with Holm correction. ***P < 0.001.

(**C**)Fluorescence changes in AAs-responsive OSNs to the vehicle, AAs, and TDT. Individual OSNs (n = 6) are represented by gray dashed lines, with the bold line and envelope indicating the mean ± SEM.

(**D**)Peak amplitude of AAs-responsive OSNs after the administration of the vehicle (black), TDT (green), and AAs (brown). One-factor repeated measures ANOVA with Holm correction. ***P < 0.001.

Fig. 5: Cell distribution in the olfactory bulb of the green spotted puffer.

(**A**) Five vertical lines (**1-5**) in the sagittal brain diagram represent the rostral-caudal positions of transverse sections of **B** - **D**. Reconstructed confocal microscopy images

of the right OB show DAPI staining in green (**B**), MAP2-immunopositive cells in magenta (**C**), and merged image (**D**). Three fish examined showed similar results. Scale bar = 100 μm

Abbreviations: **Tel**, telencephalon; **OB**, olfactory bulb; **ON**, olfactory nerve; **d**, dorsal; **v**, ventral; **l**, lateral; **m**, medial.

Fig. 6: Differential activation areas in the olfactory bulb by TDT and AAs.

Immunohistochemistry employing anti-pS6 antibody on transverse OB sections exposed to the vehicle, AAs, and TDT. (**A**) Five vertical lines (**1-5**) in the sagittal brain diagram represent the rostral-caudal positions of transverse right OB sections, which are correspondingly exposed to the vehicle(**B**), AAs(**C**), and TDT(**D**). Four fish examined for each condition showed similar results. Scale bar = 100 μm.

The density quantification of pS6-positive neurons in the dorsomedial (**dm**) and ventrolateral (**vl**) part of each section was measured (n = 4; white squares in **D5** correspond to an area of 10^4 μm^2). The rostral-caudal transition of pS6-immunopositive cell density labeled in the **dm** and **vl** part of the OB by odorant stimulations. Graphs are divided by the presented odors (**E**) or divided by **dm** or **vl** (**F**).

The same lowercase letters denote non-significant differences and different letters represent a significant difference by two-factor repeated measure ANOVA with Holm correction ($P < 0.05$).

Abbreviations: **Tel**, telencephalon; **OB**, olfactory bulb; **d**, dorsal; **v**, ventral; **l**, lateral; **m**, medial.

.

Table1: Electroporation pulse condition and GCaMP6s expression rate.

Base pulse pattern (square current pulses)

Duration(ms)	Amplitude (mA)	Frequency	Train	n	Expression rate (%)
50	0.5	10	5	6	0.09 ± 0.10

Composite pulse pattern (poring and transfer square current pulses)

Changed parameters	Interval between poring and transfer pulses	Pulse pattern	Duration(ms)	Amplitude (mA)	Frequency	Train	n	Expression rate (%)	P value: vs. Base pulse pattern (Dunnett)	P value: Pairwise comparison (Tukey)
Pattern interval	**20**	poring	5	10		1	6	0.61 ± 0.38	0.203	0.401 (vs. 100 ms)
		transfer	50	0.5	10	5				0.549 (vs. 1000 ms)
	100	poring	5	10		1	6	0.26 ± 0.20	0.879	0.962 (vs. 1000 ms)
		transfer	50	0.5	10	5				
	1000	poring	5	10		1	6	0.17 ± 0.12	0.981	
		transfer	50	0.5	10	5				
Frequency (transfer pulses)	20	poring	5	10		1	6	0.79 ± 0.29	0.358	0.906 (vs. 10 Hz)
		transfer	50	0.5	**5**	5				0.005 **(vs. 20 Hz)
	20	poring	5	10		1	6	0.61 ± 0.23	0.163	0.002 ** (vs. 20 Hz)
		transfer	50	0.5	**10**	5				
	20	poring	5	10		1	6	2.36 ± 0.41	0.00013 ***	
		transfer	50	0.5	**20**	5				
Amplitude (transfer pulses)	20	poring	5	10		1	10	1.15 ± 0.29	0.152	0.063 (vs. 1.0 mA)
		transfer	50	**0.5**	20	5				0.994 (vs. 2.0 mA)
	20	poring	5	10		1	10	2.41 ± 0.40	0.0007 ***	0.052 (vs. 2.0 mA)
		transfer	50	**1**	20	5				
	20	poring	5	10		1	10	1.10 ± 0.47	0.181	
		transfer	50	**2**	20	5				

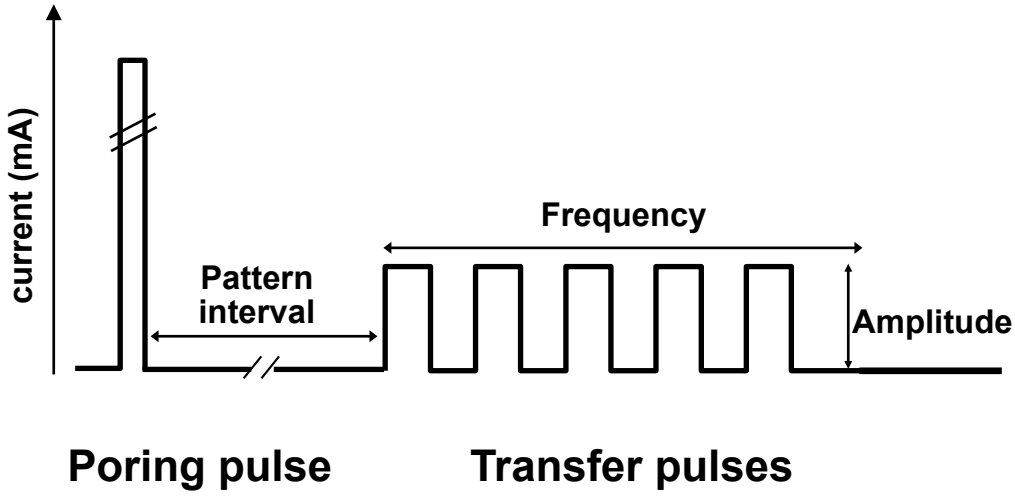
current (mA)
Frequency
Pattern
interval
Amplitude
Poring pulse
Transfer pulses

Figure 1

A

a

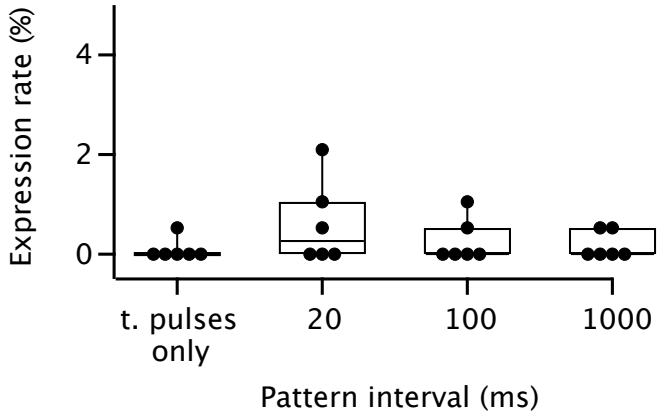

b

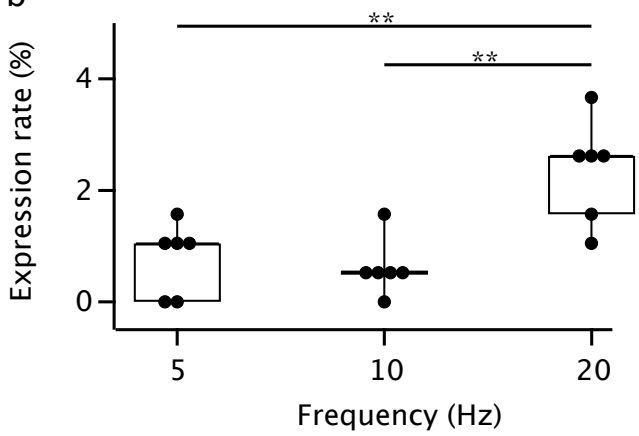

c

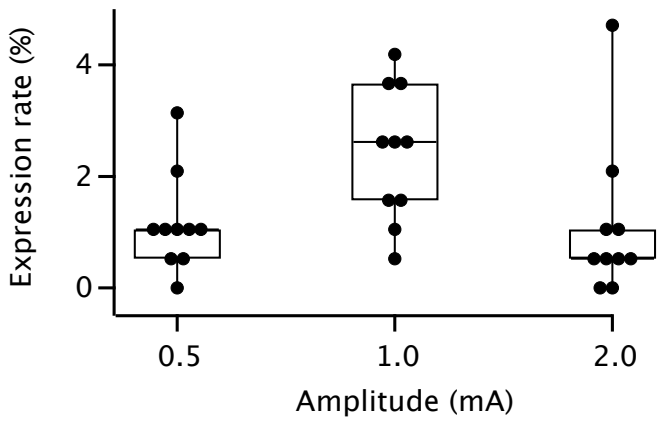

B

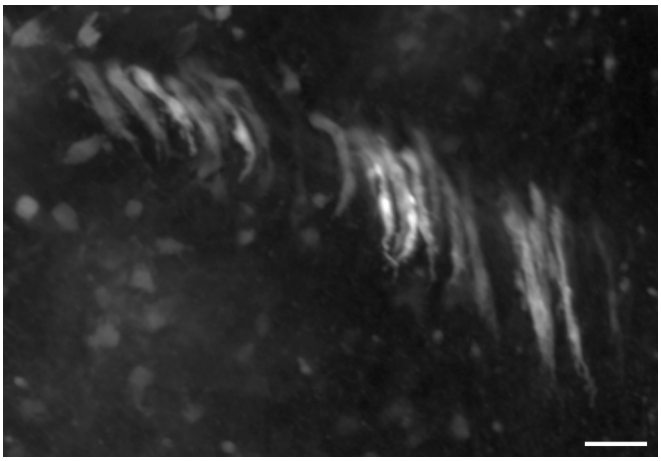

Figure 2

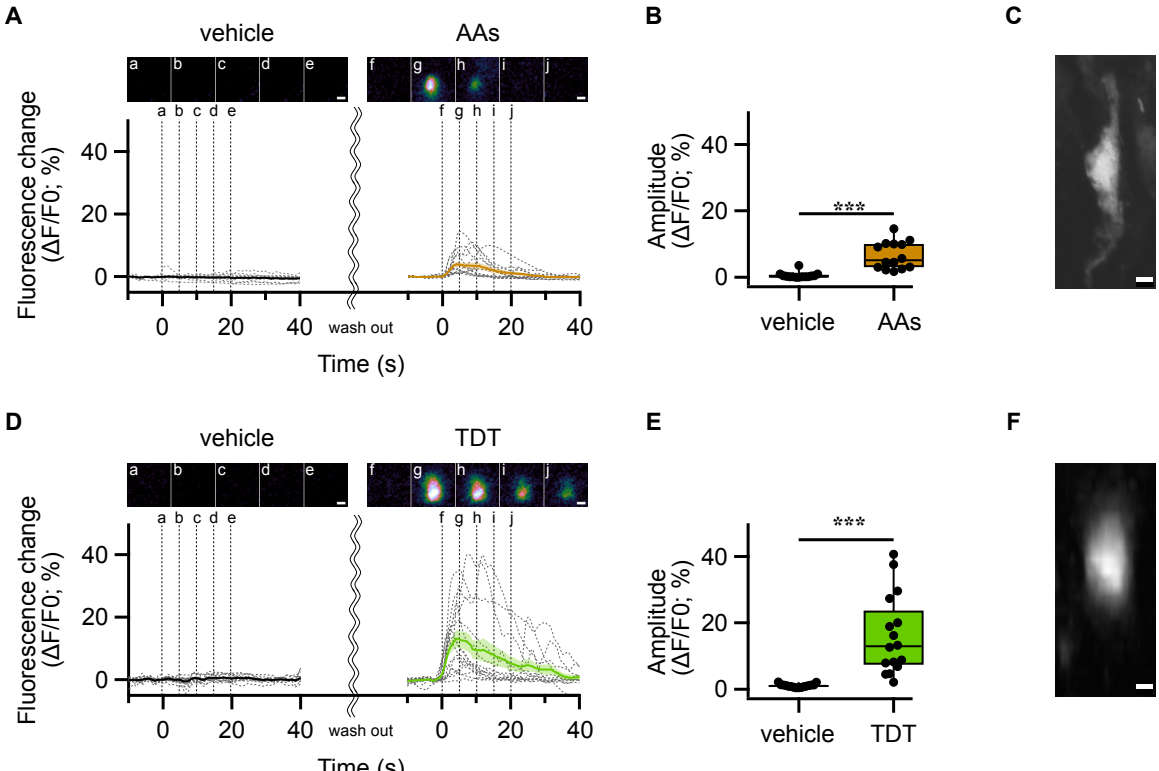
A
vehicle
AAs
a b c d e
f g h i j
Fluorescence change (ΔF/F0; %)
40
20
0
0 20 40 wash out 0 20 40
Time (s)
B
Amplitude (ΔF/F0; %)
***
vehicle
AAs
C
D
vehicle
TDT
E
Amplitude (ΔF/F0; %)
***
vehicle
TDT
F

Figure 3

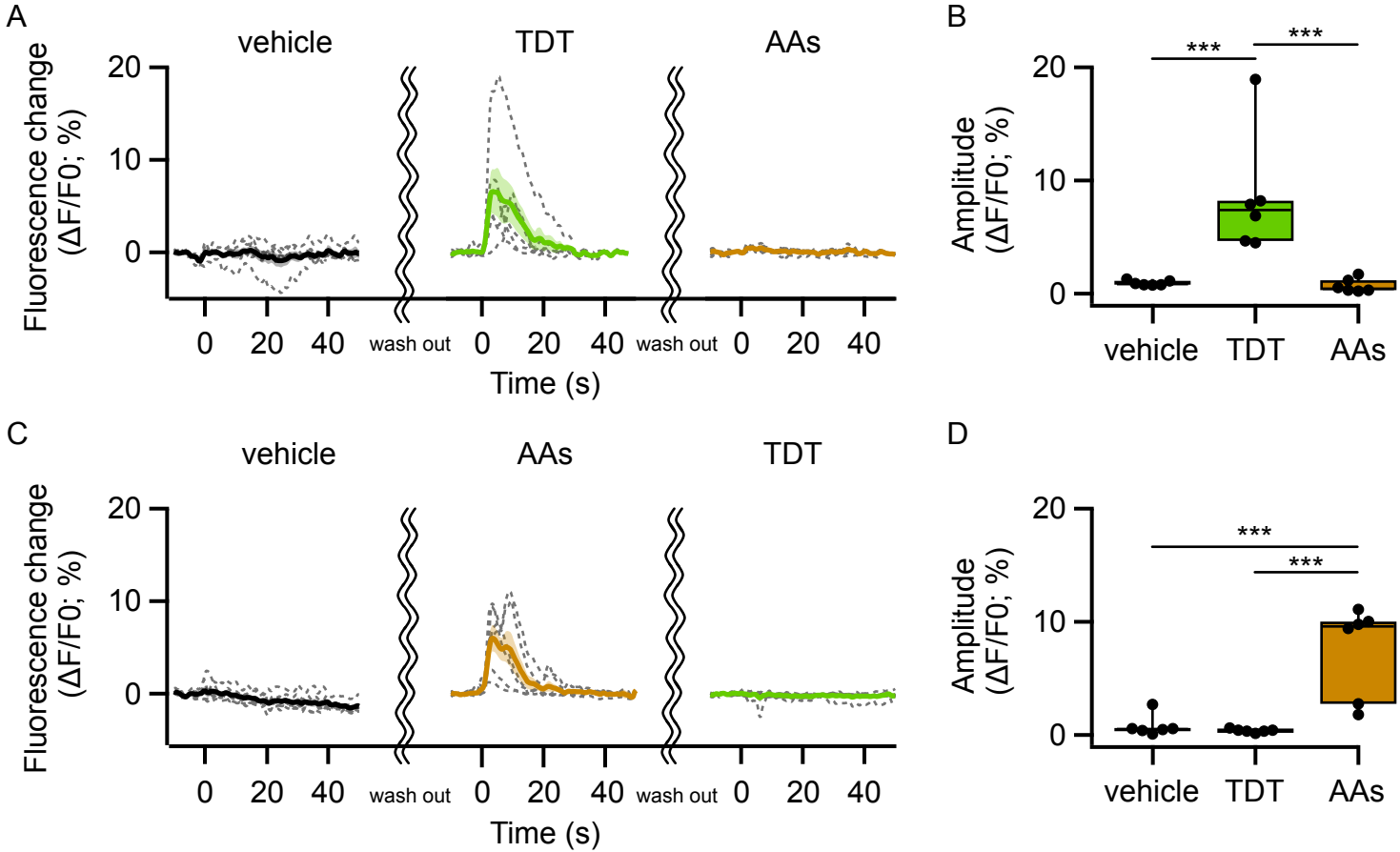
A
vehicle
TDT
AAs
Fluorescence change (ΔF/F0; %)
20
10
0
0
20
40
wash out
0
20
40
wash out
0
20
40
Time (s)
B
***
***
Amplitude (ΔF/F0; %)
20
10
0
vehicle
TDT
AAs
C
vehicle
AAs
TDT
Fluorescence change (ΔF/F0; %)
20
10
0
0
20
40
wash out
0
20
40
wash out
0
20
40
Time (s)
D
***
***
Amplitude (ΔF/F0; %)
20
10
0
vehicle
TDT
AAs

Figure 4

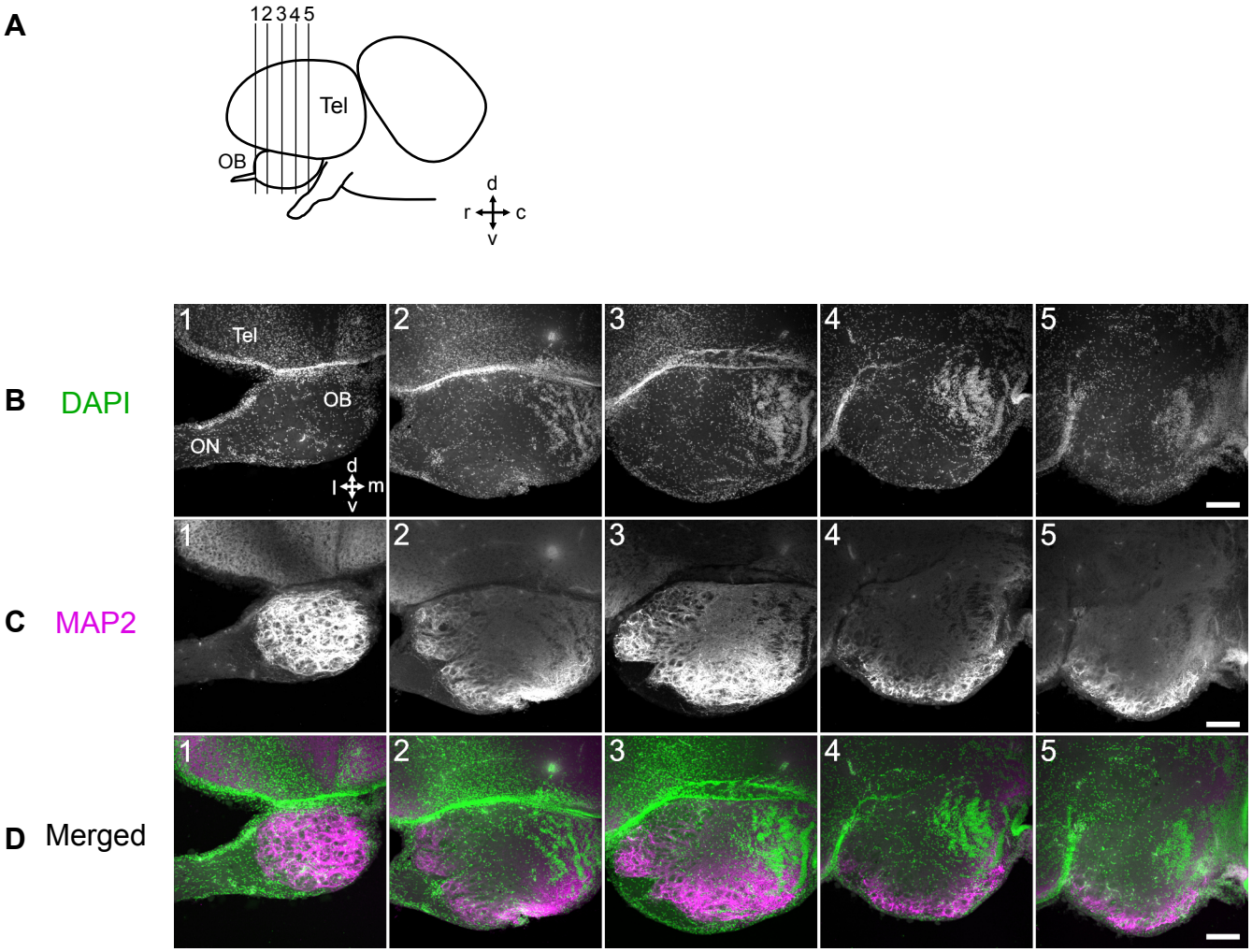

Figure 5

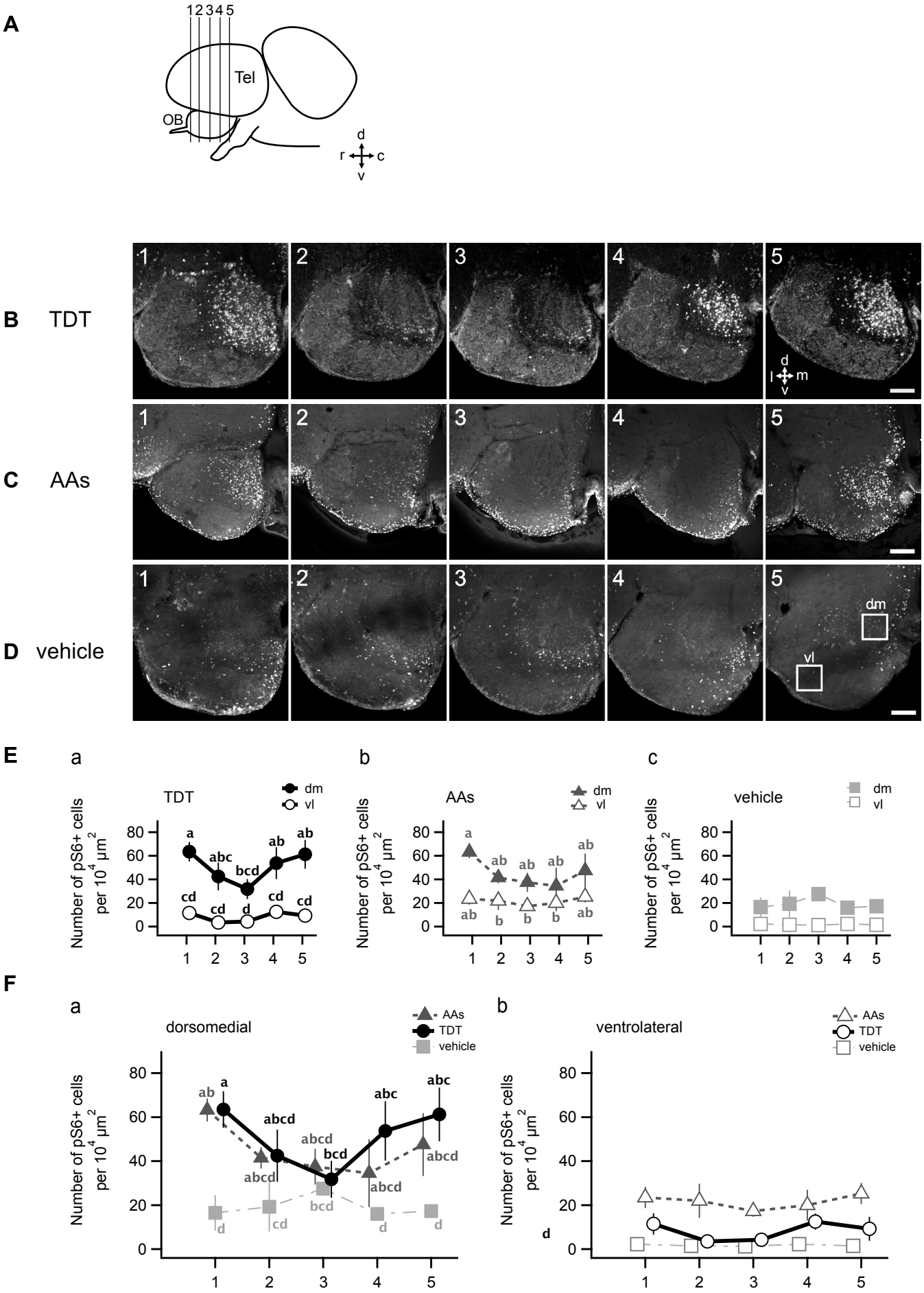
A
1 2 3 4 5
Tel
OB
d
r
c
v
B TDT
C AAs
D vehicle
1
2
3
4
5
d
l
m
v
dm
vl
E
a
b
c
TDT
AAs
vehicle
dm
vl
Number of pS6+ cells per 10^4 µm^2
F
a
b
dorsomedial
ventrolateral
AAs
TDT
vehicle

Figure 6